Controlling the properties of vortex domain walls via magnetic seeding fields

S. Hankemeier,* A. Kobs, R. Frömter, and H. P. Oepen
Institut für Angewandte Physik, Universität Hamburg, Jungiusstr. 11, 20355 Hamburg, Germany
(Received 28 April 2010; revised manuscript received 15 July 2010; published 12 August 2010)

The seeding of vortex domain walls in soft magnetic V-shaped nanowires by magnetic fields has been investigated via scanning electron microscopy with polarization analysis and micromagnetic simulations. It is found that the orientation of the magnetic seeding field determines the sense of rotation and the position of single vortex domain walls in the state of remanence. The topology of the magnetic microstructure in combination with symmetry considerations gives the key for the explanation of this behavior.

DOI: 10.1103/PhysRevB.82.064414 PACS number(s): 75.60.Ch, 75.75.−c

I. INTRODUCTION

A concept for potential applications as memory devices[1,2] is based on the micromagnetic vortex configuration, which is composed of a curling magnetization around a sharp core, where the magnetization is forced out of plane to minimize exchange energy. Stable magnetic vortices can be found as remanent state in circular microstructures as well as in nanowires as so-called vortex domain walls in head-to-head or tail-to-tail domain arrangements.[3] In microstructures it has been found that the sense of rotation of the vortex is affected by magnetic structures in the vicinity.[4–7] The ability to switch or set the sense of rotation and the polarity, i.e., the magnetization orientation of the vortex core, is a field of intense research. Recent publications demonstrate the possibility to change the sense of rotation in asymmetric single nanorings[8–10] and nanodisks[11] by applying external fields. The polarity can be manipulated via high-frequency electrical currents[12,13] or modulated magnetic fields.[14–16] While the change in vortex properties in small structures is already on the agenda of research, the seeding of vortex walls with defined properties has not yet been widely addressed. The reproducible manipulation of vortex domain wall properties is a necessary prerequisite for a storage concept based on vortex walls in combination with current-induced domain wall movement, like in the racetrack memory device.[17]

A common approach to introduce a domain wall into a V-shaped nanowire is to apply a magnetic field along the line of intersection of the two arms of the wire, which is the symmetry axis (see Fig. 1).[18,19] Depending on the direction of the external field, a head-to-head or a tail-to-tail wall nucleates at the kink as a vortex or a transverse wall depending on the dimensions of the wire.[3,20] While the influence of the seeding field on the magnetization orientation of the domains is well understood, it is still an open question what determines the vortex domain wall characteristics, i.e., the sense of rotation and position of the core with respect to the symmetry axis. For vortex walls in V-shaped wires and in wires with notches the core is slightly shifted out of the symmetry axis which is caused by the additional geometrical element,[21] while transverse walls are centered on the symmetry axis. In this paper it is demonstrated that for V-shaped wires the orientation of the seeding field is the control that determines the sense of rotation and the location of vortex walls. To investigate and explain that behavior, we have carried out experiments via scanning electron microscopy with polarization analysis[22] (SEMPA) and performed simulations with the OOMMF code.[23]

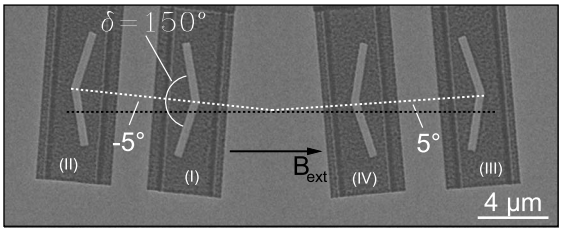

FIG. 1. Scanning electron microscope image of V-shaped wires of 400 nm width. The symmetry axis (bisection) is indicated by the white dotted line. The black arrow gives the direction of the external field used for seeding the domain walls.

II. EXPERIMENTS AND SIMULATIONS

Experimentally, V-shaped wires of 400 nm width and a bending angle of $\delta = 150°$ have been carved out of an 18 nm thick, soft magnetic $Co_{39}Fe_{54}Si_7$ (atomic percentages) film via focused ion-beam milling (Fig. 1). Figure 2 shows a SEMPA micrograph of two wires and the adjacent ferromagnetic film. The film has been grown via electron-beam

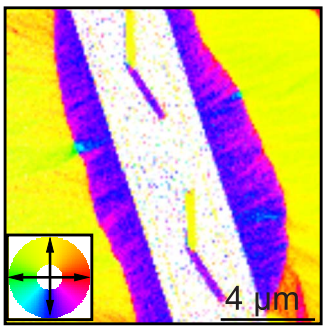

FIG. 2. (Color online) SEMPA micrograph showing two wires carved out of a continuous film via FIB milling. The orientation of the magnetization is color coded according to the color wheel. In the bright region where the ferromagnetic material has been removed no magnetic signal could be found within the uncertainty of the experiment. The adjacent film shows a domain pattern caused by the sharp edges of the structuring.

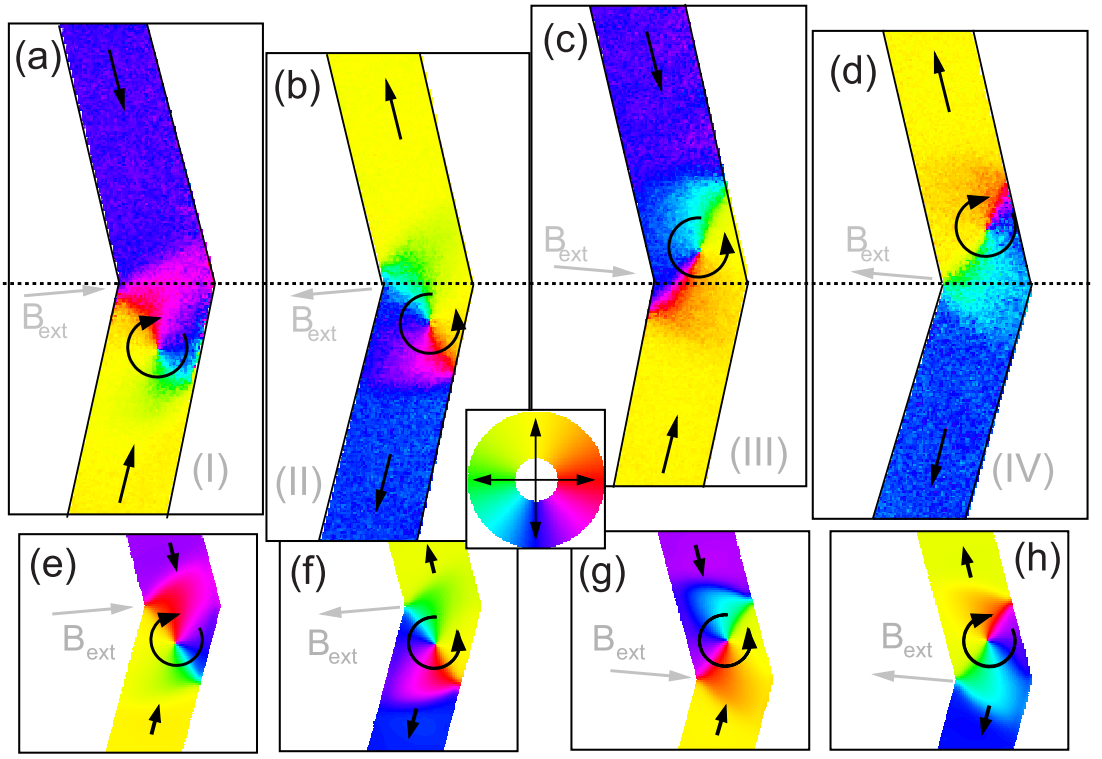

FIG. 3. (Color online) [(a)–(d)] SEMPA images of vortex domain walls in V-shaped wires after field application in the indicated directions (gray arrows). The labels (i)–(IV) refer to the four arrangements shown in Fig. 1. The orientation of the magnetization is indicated by the black arrows and color coded according to the color wheel. The images have been rotated so that the bisections of the wires are aligned with the black dotted line. In the images only the signal of the wire, i.e., within the black solid lines, is displayed. [(e)–(h)] Micromagnetic simulation of the corresponding geometries from (a)–(d) after pretreatment in an external field of B_{ext}=60 mT in the directions of the gray arrows.

evaporation on a silicon single-crystal substrate. It has been experimentally verified that the wire dimensions favor the vortex wall over the symmetric transverse wall for this film system.[24]

To investigate the influence of the orientation of the magnetic field on the vortex wall properties, wires have been created with tilt angles of ±5° [(I) and (III)] and ±175° [(II) and (IV), Fig. 1] with respect to the axis along which the magnetic field is applied in the experiment (see black arrow in Fig. 1). Such an arrangement of wires allows to investigate all four generic cases of field orientation simultaneously. To nucleate the domain walls at the bend, a magnetic seeding field of B_{ext}=60 mT is applied. After switching off the field the domain patterns of several wires were imaged via SEMPA technique with a spatial resolution of 20 nm and an angular resolution of 4°.[22] SEMPA micrographs of the predominant vortex wall structures for the four different orientations are shown in Figs. 3(a)–3(d). It has to be mentioned that no other vortex domain configuration besides the four shown in Figs. 3(a)–3(d) has been found in the experiments.

Head-to-head and tail-to-tail vortex walls are seeded depending on the direction of the magnetic field as already known from literature. The position and sense of rotation of the walls, however, depends on the exact orientation of the magnetic field. In Fig. 3(a) (B_{ext}=+60 mT at −5°) the vortex core of the head-to-head wall is moved into the lower arm and the sense of rotation is clockwise. Reversing the direction of the seeding field creates a tail-to-tail wall in remanence. The vortex core is again placed in the lower arm while the sense of rotation is switched from clockwise to counterclockwise [see Fig. 3(b)]. In Figs. 3(c) and 3(d) the orientation of the seeding field (B_{ext}= ± 60 mT) was applied at +5° with respect to the symmetry axis. The remanent configuration shows again a head-to-head/tail-to-tail wall, respectively. The vortex, however, nucleates in the upper part of the wire for both field directions. The sense of rotation again depends on the sign of the applied field, a counterclockwise/clockwise orientation is found for the two cases [Figs. 3(c) and 3(d)]. To summarize the experimental results: both the orientation of the external seeding field with respect to the symmetry axis and the sign determine which of the four micromagnetic configurations [Figs. 3(a)–3(d)] occurs. The four states can be transferred into each other by symmetry operations. A mirroring at the dashed line transfers state (a) into state (c) and (b) into (d), respectively. The states (a) and (b) can be mapped onto each other by means of a time-inversion ($\vec{M}\rightarrow-\vec{M}$, $\vec{H}\rightarrow-\vec{H}$) operation, equally (c) and (d).

We have strictly proven our results experimentally by measuring overall 47 independent domain arrangements (three *in situ* remagnetization processes). A 64% majority of all examined magnetization processes give vortex patterns that agree with the proposition for the four different vortex configurations [Figs. 3(a)–3(d)], which is a reasonable suc-

cess rate compared to similar statistics on vortex wall behavior.[5,25] A wrong vortex configuration is found with a probability of 11%, i.e., when state (a)/(b) is found instead of state (c)/(d) and vice versa. Besides vortex walls, we find transverse walls (14%) and 11% of the magnetization processes do not show a domain wall at all. Considering only the cases when vortex walls are generated the proposed structures appear with a probability of 86%.

To emphasize the experimental results we have also performed micromagnetic simulations using OOMMF.[23] We have simulated the microstructure in remanence after switching off a magnetic field of $B_{\mathrm{ext}}=\pm 60$ mT, tilted $\pm 5°$ out of the symmetry axis, corresponding to the four situations in the experiments. The micromagnetic configurations are plotted in Figs. 3(e)–3(h). The input parameters for the simulations were $M_S=1.43\times 10^6 \frac{\mathrm{A}}{\mathrm{m}}$, $A=3.5\times 10^{-11} \frac{\mathrm{J}}{\mathrm{m}}$, which agree very well with the magnetic properties of the film.[24] Further parameters for the simulations were: cell size $4\times 4\times 45$ nm^3, wire width 400 nm, thickness 45 nm, bending angle 150°, and damping constant $\alpha=0.5$. We simulated a system with higher thickness than in the experiment. The reason for this approach is to overcome the well-known problem that simulations at $T=0$ K do not necessarily find the total-energy minimum (vortex wall), as long as there exists an energy barrier to the local-energy minimum for the transverse wall.[26]

Comparing the SEMPA images [Figs. 3(a)–3(d)] and the results of the micromagnetic simulation [Figs. 3(e)–3(h), it is evident that the experiments and simulations give the same magnetic structures, i.e., the sense of rotation and position of the vortex. Even the magnetic fine structure in simulation and experiment shows the same characteristic features of the wall. Due to the high spatial resolution of the measurements, the position of the vortex core can be measured with a quite high accuracy and can be compared with the numerical investigation. The simulation gives a distance of the core to the symmetry axis of 212 nm and a lateral shift toward the outer edge of 20 nm, respectively. In the SEMPA images, we find slightly varying core positions. On the average, the SEMPA images reveal a distance of the core to the symmetry axis of 215 nm (± 50 nm) while the lateral shift is 33 nm (± 30 nm). Within the experimental uncertainty, both values are in very good agreement with the numbers found in the simulations. Thus we may conclude that the input parameters for the numerical simulation represent the experimentally studied system quite well and we can use the simulation to understand the relaxation into the zero-field magnetic configurations.

III. DISCUSSION

Before we discuss the relaxation process, we would like to recapitulate some general features of the vortex wall, which give some hint to the link between sense of rotation and wall position. Recently, the domain wall structures in soft magnetic wires were investigated from a topological point of view.[27] In the limit of preponderant magnetostatic energy it has been shown that the vortex wall consists of three topological defects. The vortex core within the wire

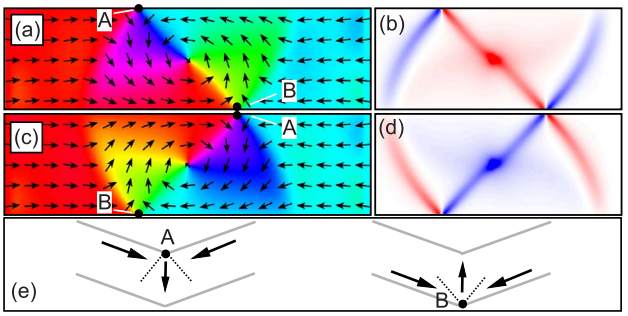

FIG. 4. (Color online) Possible configurations of a head-to-head vortex wall. In (a)/(c) the counterclockwise/clockwise configuration is displayed, respectively. The direction of magnetization is indicated by black arrows (obtained via OOMMF). In (b) and (d) the z component of the curl of the vector fields of (a) and (c) is shown, red denotes positive values, blue negative values, and white is equal to zero. In (e) a sketch of the magnetization orientation around the edge defects located at the kinks is shown.

(winding number +1) and two topological "edge defects" with winding number $-\frac{1}{2}$, i.e., two antivortex structures fixed at the edges (see Fig. 4).[28,29]

The three papers[27–29] give the key to a good understanding of details of the vortex wall structures in ultrathin, narrow wires. At first, they clearly reveal the fact that in wires the rotation of the vortex is not continuous as it is inherently conjectured form drawing the parallelism to the vortices in nanodisks. The most prominent feature of the vortex wall is a center wall that runs diagonally across the wire crossing the vortex core (Fig. 4). This wall consists of two 90° Néel walls in series with same sense of rotation connected at the core.[20] At the edges, the center wall is terminated by edge defects. Additionally, starting at the edge defects, a kind of 90° wall is built on either side of the center wall acting as borderline to the adjacent domains. The magnetization rotation across the latter borderlines gets smaller when moving from the edge defect toward the opposite side of the wire [Figs. 4(b) and 4(d)]. For the sake of clarity we call the borderlines to the adjacent domains transition lines. The center wall is tilted against the main axis of the straight wire to allow for the transition lines to start under 90° to the center wall at the edge defects. Around the edge defects the magnetization at the edge is perfectly aligned parallel to the edge of the wire preventing any stray field.

All experimental studies and simulations of vortex domain walls in small wires show these features with more or less accuracy.[3,26,30,31] Aforementioned Néel-wall-like fragments of the vortex wall are very well resolved in Lorentz microscopy studies, as the 90° walls appear as bright or dark stripes in the images.[21,32,33] As the two 90° walls building the center wall give the same contrast in the Lorentz micrographs [Figs. 4(b) and 4(d)], the center wall is usually labeled as 180° wall.

Another important feature of vortex walls in nanowires is the correlation between the tilting direction of the center wall and the sense of magnetization rotation. Not considered so far is the fact, that the symmetry of the magnetic structure fixes the location of the edge defects with respect to the

magnetization rotation around the central topological defect (vortex core). This originates from the edge defect that separates 180°-orientated magnetic structures and decomposes into two 90° domain walls at the very position of the edge defect. Changing the sense of rotation of the vortex core has the immediate consequence that the center wall will reverse its angle to the wire and the edge defects appear on the opposite edges. The two possible configurations for head-to-head walls in straight wires are shown in Fig. 4. They can be transferred into each other by mirror operation at the plane through the vortex core perpendicular to the plane of drawing and parallel/perpendicular to the wire axis, respectively. No further combination of sense of rotation and center wall tilt is possible as other combinations enforce the creation of two 180° domain walls as transition lines to the adjacent domains. Exactly the same is found for tail-to-tail walls, where the combination of sense of rotation and wall tilt is opposite to the case of head-to-head walls (time inversion). This special symmetry of head-to-head (tail-to-tail) walls is responsible for effects found in magnetotransport measurements that have been appointed to the sense of rotation.[30,34] As the sense of rotation and the tilt of the center wall lifts the high symmetry of the domain wall structure, any symmetry-breaking element (e.g., notches, kinks) in a wire will cause different pinning of the vortex wall and different properties for clockwise and counterclockwise sense of rotation.

Next we want to come back to our results of seeding domain walls in V-shaped wires. The questions that have to be answered are: why is the sense of rotation connected to the location of the core and why does the direction of the magnetic field determine both, the location and the sense of rotation?

Edge defects are very special features of the vortex wall structure. The edge defect is the location along the edge of the wire where the magnetization rotates fastest and thus contains most exchange energy. This peculiarity is the reason for an edge defect to localize at the inner kink in the case of a V-shaped wire. Here, the angle of magnetization rotation is reduced by 30° compared to a wall position in a straight wire segment and thus, exchange energy of the vortex wall configuration is most efficiently reduced. This can be made obvious by the following arguments. Imagine the two straight wire configurations of a head-to-head wall shown in Figs. 4(a) and 4(c) that nucleate in a upward bent wire. Two generic edge defects appear that can settle at the inner (A) or outer (B) edge kink. A sketch of the remaining magnetization orientation around the edge defect is shown in Fig. 4(e). Obviously, in case of settling at the outer/inner kink the rotation angle is enhanced/reduced (by 30°) as the magnetization is aligned parallel to the edge in the arms and the magnetization in the interior determines the direction of magnetization rotation. Thus, the very special structure of the edge defects causes one defect to be fixed at the inner kink due to minimization of exchange energy. The magnetostatic energy contribution of the edge defect is the same for a location at the outer or inner kink as the reduction in any pole density at the wire edges is identical. Assuming that this edge defect gives a fix point for the center wall, it remains the question in which direction the center wall will be tilted or, equivalently, what determines the sense of rotation.

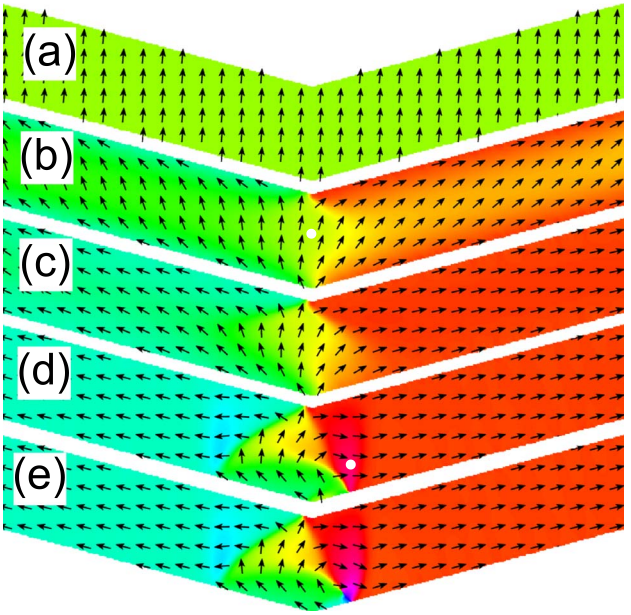

FIG. 5. (Color online) Details of the simulation of the relaxation from the fully saturated state (a) with a high damping constant of α=0.5. The field is aligned 5° toward the right-hand side of the symmetry axis. The relaxation steps shown are: (b) 50 steps, (c) 80 steps, (d) 300 steps, and (e) 400 steps. The simulation converges after 11647 steps, yielding the configuration of Fig. 3(h). The white dots are marker points which are discussed in the text.

In the following we consider just one experimental geometry as the other arrangements can be directly traced back to the described situation via symmetry considerations, as discussed above. Due to the very good accordance of simulated results and experiments it appears justified to use the relaxation steps in the micromagnetic modeling to understand the mechanism that drives the center wall into one particular direction. To reproduce the experimental situation where the magnetic field is reduced slowly compared to the intrinsic magnetodynamic time scale in the simulations, one has to reduce the field in several steps to zero using a realistic damping constant. Otherwise, unrealistic dynamical effects could influence the results. An alternative is to choose a high damping constant and switching off the field in a single step. We performed both procedures with similar results, in particular, the evolving remanent domain configuration. As the first method is very time consuming, we present the relaxation steps using the second method, where a large damping constant of α=0.5 is utilized. To demonstrate that the determination of the sense of rotation is caused by the symmetry violation of the seeding field we present the results for the starting configuration with perfectly field aligned moments.

Some of the general steps of the relaxation process are displayed in Figs. 5(a)–5(e). Figure 5(a) gives the start situation, where all moments are aligned 5° toward the right-hand side with respect to the symmetry axis (vertical direction). The relaxation is driven by the shape anisotropy which is most effectively reduced by rotating the moments into the direction parallel to the edges. The torques acting in the two arms are opposite as the angles between the moments and the edges are opposite in the field-aligned state. The rotation into

the directions along the wire axis appears at first in the vicinity of the edges (Fig. 5). The magnetization within the arm of the wire that has the smaller angle to the field direction (right-hand side) relaxes first while in the arm on the opposite side the relaxation has just started at the edges [Fig. 5(b)]. The configuration in Fig. 5(b) is quite similar to the microstructure that is achieved in a static field of $B_{\mathrm{ext}}=60$ mT. In the bend region the magnetization is preferentially oriented in the former field direction with a continuous transition to the magnetization in the arms of the wire. A slight asymmetry appears as the relaxation on the right-hand side is stronger than on the left-hand side, which pushes the transition region slightly into the left arm. Consequently, the magnetization around the symmetry axis is tilted farther to the right [see white dot in Fig. 5(b)] which is the first indication of a certain sense of rotation that is induced by the relaxation and the initial asymmetric field orientation.

In the next step [Fig. 5(c)] the magnetization in the interior of the two arms has further relaxed toward the wire axes. This relaxation step defines the transition lines and drives them closer into the bend region which causes a stronger rotation here. The sense of rotation is determined by the tendency to keep the magnetization parallel to the edges while around the symmetry axis nearly no shape-induced torque is effective. Here the magnetization rotates to establish the continuous transition between the oppositely magnetized arms while the former sense of rotation is maintained and the asymmetry is even enhanced. In the next step [Fig. 5(d)] the transition line on the right-hand side continues to move into the bend region while the magnetization rotation appears also across the transition line [see white dot in Fig. 5(d)]. At this step the sense of rotation of the vortex is clearly visible and the first structure that tags the center wall is established. As the sense of rotation and the tilting of the center wall are strongly correlated (see above), the center wall has to move into the right arm, as the edge defect has to settle at the inner kink. Next [Fig. 5(e)], a combined vortex core/edge defect is created at the end of the sharp transition line on the right-hand side, thus generating all structures needed for the center wall. Finally, vortex core and edge defect separate and the center wall is pushed further away from the bend region to allow for the second 90° segment at the edge defect to form, acting as transition line to the domain in the arm on the right-hand side [Fig. 3(h)]. In contrast, the transition line on the left-hand side is almost unchanged, during relaxation after the step shown in Fig. 5(c).

In brief, the driving force of the relaxation process stems from the shape anisotropy that acts first on the moments at the edges. Inside the bend region the net torque is vanishingly small or the opposite torques on both sides compensate, which lets the moments stay almost in the field-aligned orientation, e.g., toward the right-hand side. The shape-aligned moments along the edges and the former field-aligned moments in the bend region then define the sense of rotation of the vortex. As the sense of rotation and the tilt of the center wall are linked, the vortex core settles in the arm that is closer to the seeding field direction.

The core nucleation process [Fig. 5(e)] was predicted from topologic considerations for the reversed case, the annihilation of the center wall with field.[29] In Ref. 29 the transition from a vortex wall to a transverse wall is postulated. We find a transition of a transverse-wall-like configuration into the vortex wall during the relaxation process, when the same simulation is carried out for a reduced wire width (e.g., 300 nm), where the transverse wall becomes energetically more favorable and can be clearly observed during the relaxation process.

The results presented here are not limited to the discussed geometry. They can be seen as a more universal behavior for the seeding of vortex walls in bent nanowires in a particular span of geometries. At first, vortex walls must be energetically more favorable than transverse walls which depends on the wire dimensions[26] as well as on the bending angle.[24] The tilting angle of the seeding field θ with respect to the symmetry axis is limited. The lower bound is given by the fact that the symmetry has to be broken, i.e., $\theta>0°$. The upper bound is determined by the torques in the arms, which have to be oppositely oriented, i.e., $\theta<90°-\frac{\delta}{2}$ (with bending angle δ). For larger θ domain walls cannot be nucleated.

IV. CONCLUSION

Following the general considerations about topology we find that the symmetry of the vortex head-to-head (tail-to-tail) domain walls allows for two generic geometries only. The two principal vortex structures have an opposite sense of rotation that is inherently connected to an opposite tilting angle of the center wall to the wire axis (Fig. 4). This symmetry property of vortex domain walls is the key link to the understanding of the behavior of the vortex wall in V-shaped wires. By means of SEMPA investigations and micromagnetic simulations it is shown that the sense of rotation/location of the vortex wall in V-shaped wires can be tuned via magnetic fields that are slightly tilted out of the symmetry axis of the wire. The simulations allow for an understanding of the relaxation process which reveals that the shape anisotropy-induced relaxation in the arms and the field alignment in the bend region fix the sense of rotation in the beginning of the relaxation process. The possibility to purposely control the sense of rotation and the polarity of a vortex domain wall gives more flexibility in future concepts of vortex-based memory devices. A V-shaped injection wire can be used to define a single vortex configuration which acts as a four-state bit element and can be moved into a memory array utilizing the spin torque effect, in analogy to the working principle of the racetrack memory.[17]

ACKNOWLEDGMENT

Financial support by DFG via SFB 668 is gratefully acknowledged.

*shankeme@physnet.uni-hamburg.de

[1] R. P. Cowburn, Nature Mater. **6**, 255 (2007).
[2] S. Bohlens, B. Krüger, A. Drews, M. Bolte, G. Meier, and D. Pfannkuche, Appl. Phys. Lett. **93**, 142508 (2008).
[3] A. Thiaville, Y. Nakatani, F. Piéchon, J. Miltat, and T. Ono, Eur. Phys. J. B **60**, 15 (2007).
[4] S. Y. H. Lua, S. S. Kushvaha, Y. H. Wu, K. L. Teo, and T. C. Chong, Appl. Phys. Lett. **93**, 122504 (2008).
[5] M. Konoto, T. Yamada, K. Koike, H. Akoh, T. Arima, and Y. Tokura, J. Appl. Phys. **103**, 023904 (2008).
[6] S. Hankemeier, R. Frömter, N. Mikuszeit, D. Stickler, H. Stillrich, S. Pütter, E. Y. Vedmedenko, and H. P. Oepen, Phys. Rev. Lett. **103**, 147204 (2009).
[7] T. J. Hayward, M. T. Bryan, P. W. Fry, P. M. Fundi, M. R. J. Gibbs, M.-Y. Im, P. Fischer, and D. A. Allwood, Appl. Phys. Lett. **96**, 052502 (2010).
[8] W. Jung, F. J. Castano, and C. A. Ross, Phys. Rev. Lett. **97**, 247209 (2006).
[9] R. Nakatani, T. Yoshida, Y. Endo, Y. Kawamura, M. Yamamoto, T. Takenaga, S. Aya, T. Kuroiwa, S. Beysen, and H. Kobayashi, J. Appl. Phys. **95**, 6714 (2004).
[10] M. Kläui, J. Rothman, L. Lopez-Diaz, C. A. F. Vaz, J. A. C. Bland, and Z. Cui, Appl. Phys. Lett. **78**, 3268 (2001).
[11] Y. Gaididei, D. D. Sheka, and F. G. Mertens, Appl. Phys. Lett. **92**, 012503 (2008).
[12] K. Yamada, S. Kasai, Y. Nakatani, K. Kobayashi, H. Kohno, A. Thiaville, and T. Ono, Nature Mater. **6**, 270 (2007).
[13] Y. Liu, S. Gliga, R. Hertel, and C. M. Schneider, Appl. Phys. Lett. **91**, 112501 (2007).
[14] R. Hertel, S. Gliga, M. Fähnle, and C. M. Schneider, Phys. Rev. Lett. **98**, 117201 (2007).
[15] D. J. Keavney, X. M. Cheng, and K. S. Buchanan, Appl. Phys. Lett. **94**, 172506 (2009).
[16] M. Weigand, B. Van Waeyenberge, A. Vansteenkiste, M. Curcic, V. Sackmann, H. Stoll, T. Tyliszczak, K. Kaznatcheev, D. Bertwistle, G. Woltersdorf, C. H. Back, and G. Schütz, Phys. Rev. Lett. **102**, 077201 (2009).
[17] S. S. P. Parkin, M. Hayashi, and L. Thomas, Science **320**, 190 (2008).
[18] T. Taniyama, I. Nakatani, T. Namikawa, and Y. Yamazaki, Phys. Rev. Lett. **82**, 2780 (1999).
[19] T. Taniyama, I. Nakatani, T. Yakabe, and Y. Yamazaki, Appl. Phys. Lett. **76**, 613 (2000).
[20] R. McMichael and M. Donahue, IEEE Trans. Magn. **33**, 4167 (1997).
[21] C. Brownlie, S. McVitie, J. N. Chapman, and C. D. W. Wilkinson, J. Appl. Phys. **100**, 033902 (2006).
[22] R. Frömter, S. Hankemeier, H. P. Oepen, and J. Kirschner (unpublished).
[23] M. Donahue and D. Porter, National Institute of Standards and Technology Interagency Report No. NISTIR 6376, 1999 (unpublished).
[24] A. Kobs, S. Hankemeier, R. Frömter, and H. P. Oepen (unpublished).
[25] D. Backes, C. Schieback, M. Kläui, F. Junginger, H. Ehrke, P. Nielaba, U. Rüdiger, L. J. Heyderman, C. S. Chen, T. Kasama, R. E. Dunin-Borkowski, C. A. F. Vaz, and J. A. C. Bland, Appl. Phys. Lett. **91**, 112502 (2007).
[26] M. Kläui, J. Phys.: Condens. Matter **20**, 313001 (2008).
[27] O. Tchernyshyov and G.-W. Chern, Phys. Rev. Lett. **95**, 197204 (2005).
[28] G.-W. Chern, H. Youk, and O. Tchernyshyov, J. Appl. Phys. **99**, 08Q505 (2006).
[29] H. Youk, G.-W. Chern, K. Merit, B. Oppenheimer, and O. Tchernyshyov, J. Appl. Phys. **99**, 08B101 (2006).
[30] M. Hayashi, L. Thomas, C. Rettner, R. Moriya, X. Jiang, and S. S. P. Parkin, Phys. Rev. Lett. **97**, 207205 (2006).
[31] W. C. Uhlig, M. J. Donahue, D. T. Pierce, and J. Unguris, J. Appl. Phys. **105**, 103902 (2009).
[32] D. McGrouther, S. McVitie, J. N. Chapman, and A. Gentils, Appl. Phys. Lett. **91**, 022506 (2007).
[33] K. J. O'Shea, S. McVitie, J. N. Chapman, and J. M. R. Weaver, Appl. Phys. Lett. **93**, 202505 (2008).
[34] E.-S. Wilhelm, D. McGrouther, L. Heyne, A. Bisig, and M. Kläui, Appl. Phys. Lett. **95**, 252501 (2009).